The Astrophysical Journal Letters, 893:L18 (5pp), 2020 April 10 https://doi.org/10.3847/2041-8213/ab8566

Formation of Macroscale Flux Transfer Events at Mercury

J. Zhong[1], Y. Wei[1], L. C. Lee[2,3], J. S. He[4], J. A. Slavin[5], Z. Y. Pu[4], H. Zhang[1], X. G. Wang[6], and W. X. Wan[1]
[1] Key Laboratory of Earth and Planetary Physics, Institute of Geology and Geophysics, Chinese Academy of Sciences, Beijing, People's Republic of China
[2] Institute of Earth Sciences, Academia Sinica, Taipei, Taiwan
[3] State Key Laboratory of Lunar and Planetary Sciences, Macau University of Science and Technology, Macau, People's Republic of China
[4] School of Earth and Space Sciences, Peking University, Beijing, People's Republic of China
[5] Department of Climate and Space Sciences and Engineering, University of Michigan, Ann Arbor, MI, USA
[6] Department of Physics, Harbin Institute of Technology, Harbin, People's Republic of China
Received 2020 March 17; accepted 2020 March 31; published 2020 April 13

Abstract

Flux transfer events (FTEs) are magnetic flux ropes that are produced via magnetic reconnection at the planetary magnetopause where the solar wind directly interacts with the magnetosphere. Previous observations show that FTEs with a duration of several seconds, corresponding to a spatial scale of ∼0.5–1 R_M, can occur at Mercury. However, the formation of these macroscale FTEs at a small dimensional magnetopause with a radius of ∼1.5 R_M remains unclear. Here, we report the observations of active magnetic reconnection events at Mercury's magnetopause by the MESSENGER spacecraft. The reconnection process is dominated by the formation of a series of multi-scale FTEs. Ion-scale flux ropes, typically with durations of ∼1 s or less, may be produced by the tearing instability in the thin current sheet near the subsolar position. Moreover, the commonly observed macroscale FTEs consist of three to tens of successive small-scale FTEs. We propose that macroscale FTEs at Mercury are generated by the interaction and merging of multiple ion-scale flux ropes, probably through two or more steps. This is distinct from the formation of typical FTEs, mainly between a pair of X-lines, at Earth's magnetopause. Thus, the formation and evolution of FTEs may differ among planetary magnetospheres with a vast range of scale sizes. We further conclude that Mercury's magnetopause is a natural plasma laboratory to study flux rope dynamics and evolution for the upcoming Bepi-Colombo mission.

Unified Astronomy Thesaurus concepts: Planetary magnetosphere (997); Mercury (planet) (1024); Solar magnetic reconnection (1504); Planetary boundary layers (1245); Solar-planetary interactions (1472)

1. Introduction

Magnetic flux ropes are ubiquitous magnetic reconnection features throughout the heliosphere. At the magnetopause, flux ropes, termed flux transfer events (FTEs), topologically connect the interplanetary and planetary magnetic fields (Russell & Elphic 1978). They provide an efficient coupling between the solar wind and magnetospheres. Typical FTEs at Earth are on a spatial scale of one to a few R_E (where 1 R_E = 6400 km), with time durations of ∼0.5 minute (e.g., Wang et al. 2005). It is widely accepted that FTEs, with their characteristic flux rope structure, are produced between two simultaneous, or sequential, reconnection X-lines at the magnetopause (e.g., Lee & Fu 1985; Raeder 2006; Hasegawa et al. 2010; Øieroset et al. 2011; Zhang et al. 2012; Pu et al. 2013; Zhong et al. 2013). FTEs have also been discovered at other magnetized planetary magnetopauses, such as those of Mercury (Russell & Walker 1985), Saturn (Jasinski et al. 2016), and Jupiter (Walker & Russell 1985), and proposed to occur in the heliopause (Schwadron & McComas 2013). Given the distinct magnetopause scales and plasma environments, the behavior of the reconnection and, consequently, the formation and evolution of FTEs may differ among various planets.

Mercury has the smallest planetary magnetosphere in our solar system, resulting from its relatively weak planetary magnetic field compressed by the intense solar wind in the inner heliosphere. The dimension of the dayside magnetopause, or its subsolar distance, is only approximately 1.5 R_M (where R_M is Mercury's radius, 2440 km; e.g., Zhong et al. 2015a, 2015b). The high solar wind Alfvén velocity at Mercury's orbit makes the reconnection more efficient than that at Earth and other magnetized planets (Slavin et al. 2009; Zhong et al. 2018). Typical FTEs observed at Mercury have durations of ∼1 s or less and reoccur in ∼10 s (e.g., Russell & Walker 1985; Slavin et al. 2012, 2014). Their mean diameters were estimated to be ∼300–400 km, or ∼10% of the magnetopause subsolar distance, which is similar to the relative dimensions of terrestrial FTEs. Furthermore, individual macroscale FTEs with a duration of several seconds, on a corresponding spatial scale of ∼0.5–1 R_M, were also observed at Mercury (Slavin et al. 2010; Imber et al. 2014). They can carry a large quantity of magnetic flux and play a crucial role in driving the magnetospheric flux circulation (Imber et al. 2014). However, their large diameters pose a problem with regard to their single-step formation via multiple X-line reconnection at a magnetopause with a radius of ∼1.5 R_M. Most reported macroscale FTEs were identified in Mercury's magnetosheath and far from the reconnection region. Moreover, the lack of any ongoing reconnection signatures indicates that they were mature and not observed during their formation or active stage.

Here, we report two active reconnection events at Mercury's dayside magnetopause observed by the MESSENGER spacecraft. The observations suggest that the macroscale FTEs can be formed through the interaction and merging of multiple small-scale flux ropes that probably generated near the reconnection site at the subsolar magnetopause. The formation and evolution of these macroscale FTEs may play an important

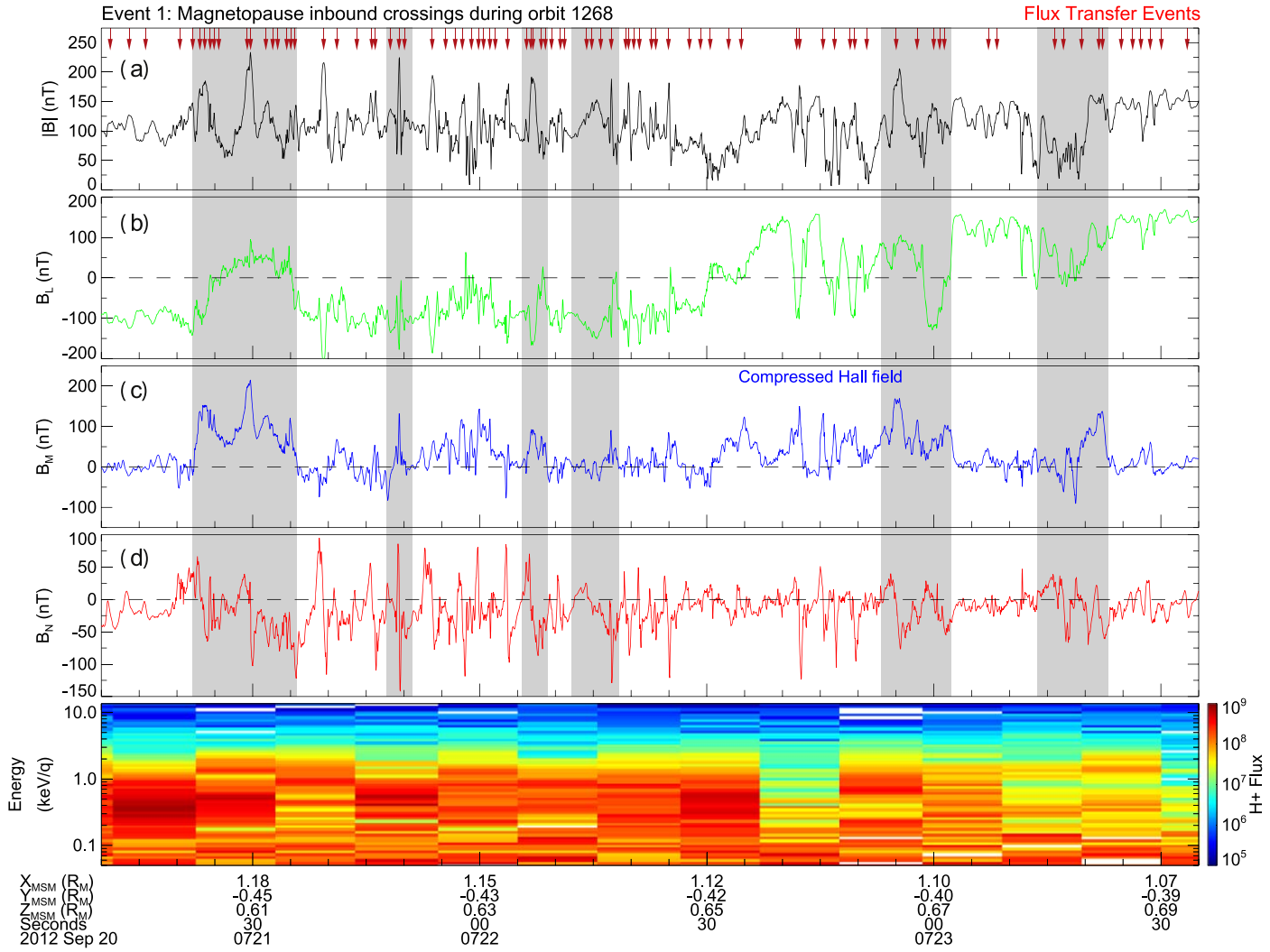

Figure 1. MESSENGER observations of the active reconnection at Mercury's magnetopause on 2012 September 20. (a)–(d) Magnetic field magnitude and its three components in the *LMN* coordinates. Relative to the aberrated Mercury solar-magnetospheric (MSM) coordinate system, $L = (-0.49, 0.34, 0.80)$, $M = (-0.22, -0.94, 0.26)$, and $N = (0.84, -0.05, 0.54)$. (e) Spectrogram of the ion differential energy flux ($cm^{-2}\ Sr^{-2}\ s^{-1}\ eV^{-1}$). Red arrows mark the occurrence of FTEs with durations longer than 0.5 s. The shaded regions indicate the possible interaction and merging of multiple small-scale FTEs.

role in regulating Mercury's exosphere and thus in the magnetosphere–exosphere–surface coupling.

2. Observations

We use the high-resolution magnetic field data (20 samples s^{-1}) from the Magnetometer (MAG) instrument (Anderson et al. 2007) and the proton flux data from the Fast Imaging Plasma Spectrometer (FIPS) instrument (Andrews et al. 2007). Figures 1 and 2 present the observations of two active reconnection events during the crossing of the magnetopause on 2012 September 20 (Event 1) and 2013 May 31 (Event 2), respectively. The magnetic field data were analyzed in a local current sheet coordinate system (*LMN*), determined from the minimum variance analysis of the magnetic field across the magnetopause, with *N* along the direction normal to the overall current sheet pointing outward, *L* along the reconnecting component of the magnetic field pointing northward, and *M* along the guide field (X-line) direction pointing dawnward. For both events, the spacecraft crossed the magnetopause in the middle magnetic latitude of the north hemisphere from the magnetosheath side ($B_L < 0$ and high proton flux) to the magnetospheric side ($B_L > 0$ and low proton flux). The heated magnetosheath ions detected during the two events indicate that the spacecraft remained in the magnetopause boundary layer.

The two reconnection events are characterized by the formation of numerous multi-scale FTEs. The FTE structures can be identified by the bipolar signature in the B_N component and are typically coincident with the enhancements of B_M and $|B|$. Here, we identified the FTEs with durations longer than 0.5 s, as marked by the red arrows in Figures 1 and 2. The B_N positive-to-negative polarity indicates that they were all moving northward from the subsolar region. For a typical dayside magnetosheath flow of $\sim$300 km s^{-1}, the FTEs with durations of $\sim$1 s correspond to the ion-scale structures. By comparison, the gyroradius of a 1 keV magnetosheath proton in the 100 nT magnetic field is $\sim$50 km. There were 86 FTEs in Event 1 and 72 FTEs in Event 2, both occurring within an interval of 145 s. The average re-occurrence time is $\sim$1.7 and $\sim$2 s, respectively, indicating that they are proximal to each other. Note that frequent FTEs, which are termed as "FTE showers," were previously observed at the tail magnetopause (Slavin et al. 2012, 2019).

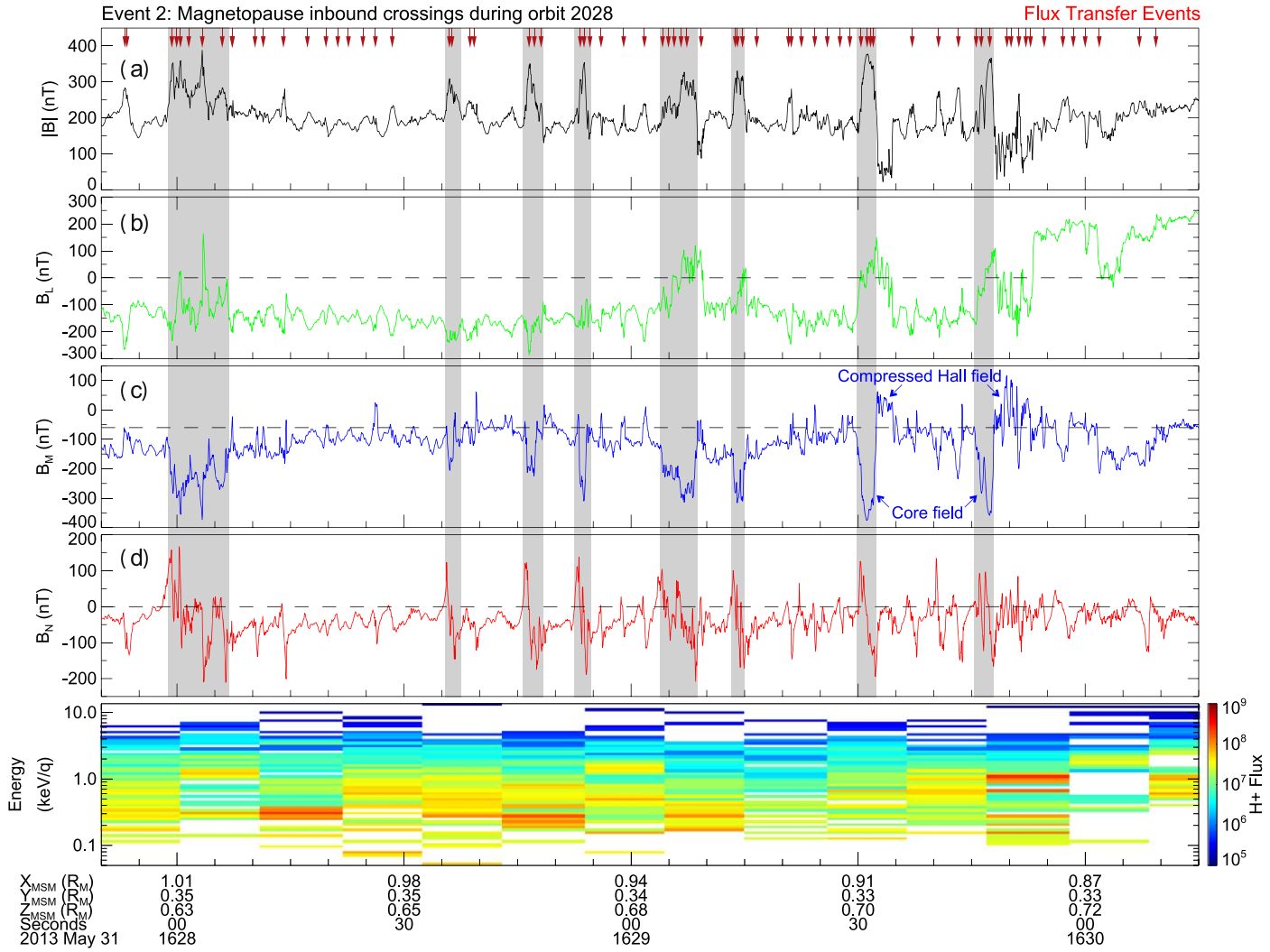

Figure 2. MESSENGER observations of the active reconnection at Mercury's magnetopause on 2013 May 31. (a)–(d) Magnetic field magnitude and its three components in the *LMN* coordinates. Relative to the aberrated MSM coordinate system, $L = (-0.53, -0.53, 0.67)$, $M = (0.36, -0.85, -0.38)$, and $N = (0.77, 0.04, 0.64)$. (e) Spectrogram of the ion differential energy flux (cm^{-2} Sr^{-2} s^{-1} eV^{-1}). See Figure 1 for other information.

The interaction and merging of multiple flux ropes are common features in the simulations of flux-rope–dominated current sheet (e.g., Markidis et al. 2012; Zhou et al. 2014). The gray shaded regions in Figures 1 and 2 show the possible interaction and merging of multiple small-scale FTEs into macroscale FTEs. Their durations are from ~2 to ~14 s. The size of these macroscale FTEs can be estimated as ~0.3–1.7 R_M along the magnetopause. Figure 3 shows a close-up view of typical macroscale FTEs in Event 2. The 1 s smoothed data show clear large bipolar B_N structures for each merged structure. Their whole bipolar B_N actually consisted of multiple successive short-duration asymmetric bipolar variations. Such a behavior of the magnetic field is consistent with the interaction and merging of multiple flux ropes in the numerical simulations (e.g., Zhou et al. 2014).

The flux rope merging events have been previously observed in geospace (e.g., Wang et al. 2015; Zhou et al. 2017) and in the coronal mass ejection event (e.g., Song et al. 2012; Feng et al. 2019; Gou et al. 2019), but they commonly occur between a pair of flux ropes. Here, multiple flux ropes interaction and merging at Mercury's magnetopause lead to much more complicated inner structures. As shown in Figure 3, at least four, three, 10, and three small-scale FTEs are found inside macroscale FTE1, FTE2, FTE3, and FTE4, respectively. From the smoothed data, it can be observed that FTE3 actually exhibits a weak and narrow inner negative-to-positive B_N bipolar structure. Such a magnetic feature has been demonstrated by high-quality data from the MMS spacecraft as the dissipation or erosion of magnetic field via reconnection between two flux ropes (Zhou et al. 2017). Similar macroscale complicated structures of FTEs were also observed during 16:27:58–16:28:07 UT in Event 2 and during 07:21:22–07:21:36 UT in Event 1. These findings suggest that the FTEs may grow into macroscales through interaction and merging via two or more steps.

The core field of the FTEs can be a result of the compression of the guide field and/or Hall magnetic field (e.g., Wang et al. 2015). The signatures of the reconnection Hall magnetic field during the current sheet crossings are expected to be observed in the B_M components. Previous observations at Earth's magnetopause suggest that the Hall magnetic fields are shifted toward and enhanced on the magnetosheath side (positive/negative in the north/south of the X-line) and reduced or disappeared in the magnetospheric side, owing to the

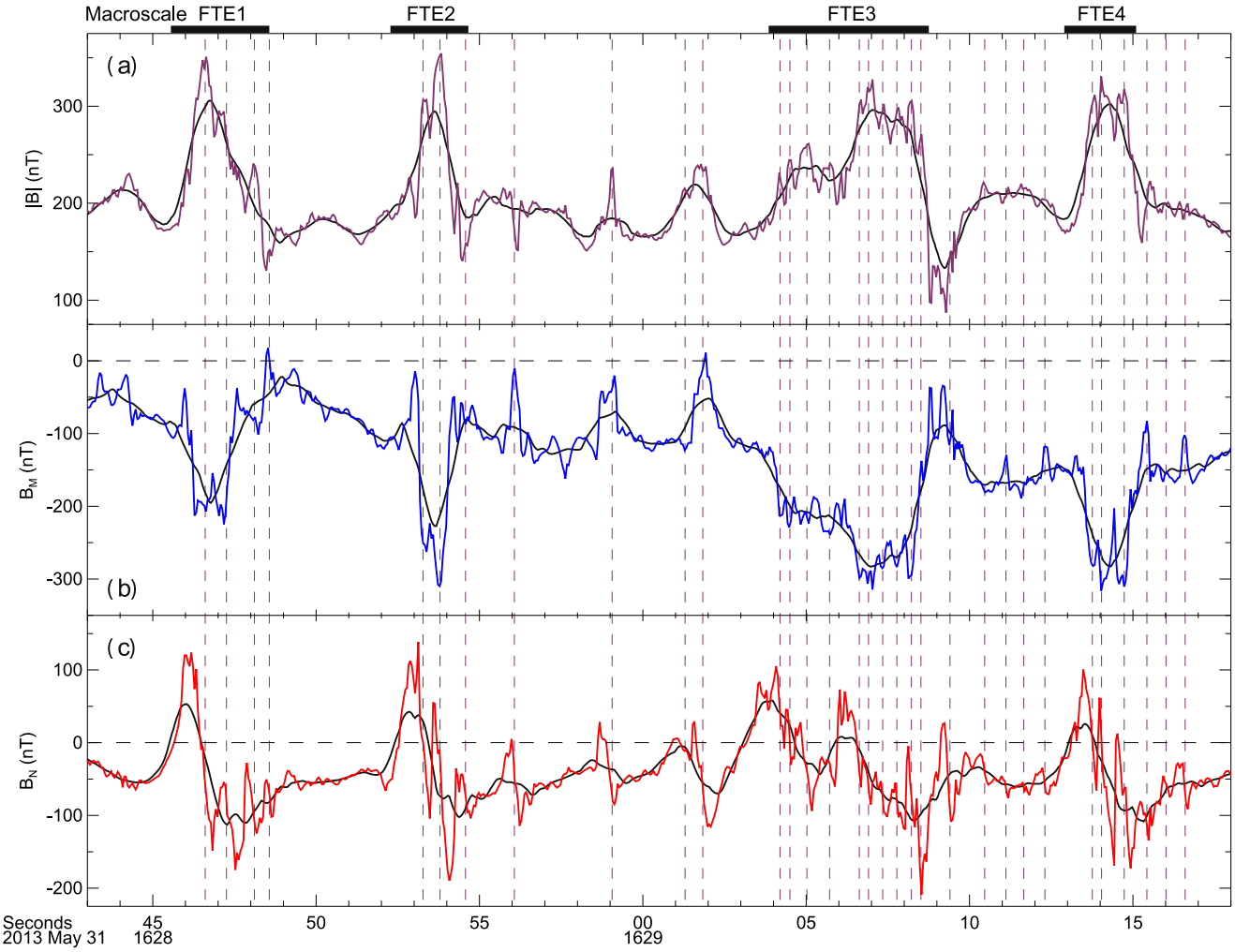

Figure 3. Close-up view of the macroscale FTEs in Event 2. (a) Magnetic field magnitude. (b) B_M. (c) B_N. Vertical purple dashed lines are identified as small-scale FTEs. Black lines are smoothed magnetic field, created by performing boxcar averaging on the magnetic field data using a 1 s window, and used for identifying macroscale FTE1–FTE4, marked above the figure.

asymmetry in plasma density across the magnetopause (e.g., Tanaka et al. 2008; Zhang 2016; Wang et al. 2017). During the magnetopause crossing on 2012 September 20 (Figure 1), the magnetic shear between the magnetosheath and magnetosphere is nearly anti-parallel, and the guide field $B_g \approx 0$ nT. The overall positive B_M across the current sheet is consistent with that of the Hall magnetic field northward the X-line at the magnetopause. The presence of a strong positive core field inside the FTEs may result from the compression of the Hall magnetic field. On 2013 May 31 (Figure 2), the guide field $B_g \approx -60$ nT, or $\sim$30% B_L, suggesting a guide field reconnection event. The $(B_M - B_g)$ value is also overall positive across the current sheet. The strong negative core field of the macroscale FTEs may result from the compression of the guide field. Moreover, such FTEs are surrounded by positive $(B_M - B_g)$, or Hall magnetic field, perturbations. These possible Hall magnetic field signatures further suggest that the reconnection is ongoing and that the macroscale FTEs are in their formation and evolution stage.

3. Discussion

We have presented the observations of active magnetic reconnection characterized by the formation of highly frequent FTEs with different scales at Mercury's dayside magnetopause. The macroscale FTEs consist of numerous small-scale FTEs, leading to complex inner structures. The observations suggest that the interaction and merging of multiple flux ropes are common features of Mercury's magnetopause that can occur under both anti-parallel and component reconnection. At Earth, large FTEs can be formed via dual or multiple sequential X-line reconnection, owing to the presence of a geomagnetic dipole tilt (Raeder 2006). By contrast, Mercury has nearly no dipole tilt (Anderson et al. 2012). The reconnection processes are thus expected to be continuous on the subsolar magnetopause. The intense solar wind dynamic pressure compression at Mercury's magnetopause causes the current sheet to become very thin, which allows the development of the tearing instability and thus the production of multiple ion-scale flux ropes or FTEs (Lee & Fu 1986). Small flux ropes can also be formed through the secondary instabilities in the vicinity of the reconnection site (e.g., Drake et al. 2006; Daughton et al. 2011). As these small-scale FTEs are ejected and propagate away from the reconnection sites, they may grow, decelerate, contact with one another, and merge into macroscale FTEs, as shown in Figure 4.

In a three-dimensional configuration, these FTEs are connecting, or at least partially connecting, the interplanetary

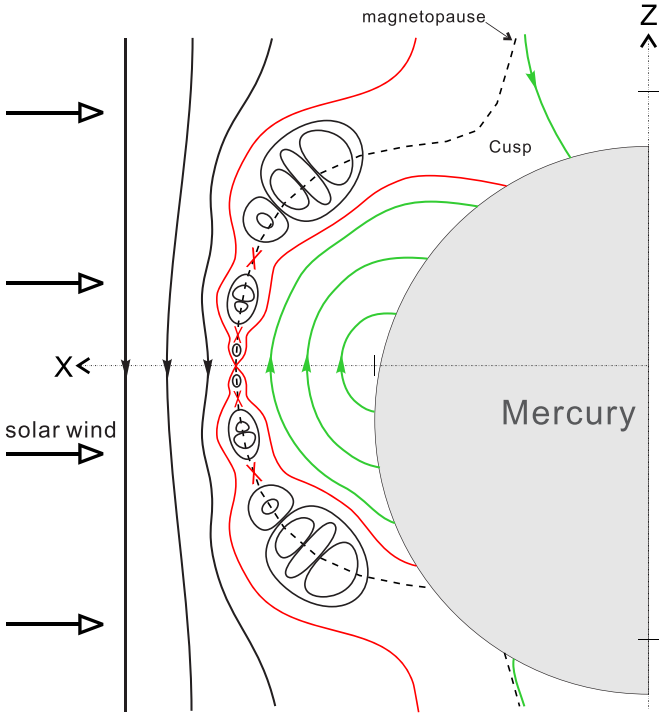

Figure 4. Schematic of macroscale flux transfer events formed at Mercury's dayside magnetopause.

magnetic field to the surface of the planet, similar to those of the Earth (e.g., Lee et al. 1993; Pu et al. 2013; Zhong et al. 2013). The solar wind plasma can move along the field line and directly impact Mercury's surface without the obstacle of an appreciable atmosphere, leading to ion sputtering and then influencing the global exosphere environment (e.g., Milillo et al. 2005; Orsini et al. 2007). The formation and evolution of macroscale FTEs at the magnetopause may regulate Mercury's exosphere and thus the magnetosphere–exosphere–surface coupling. The investigation of magnetopause reconnection, flux rope dynamics, and their effect on the regulation of Mercury's space environment will be enabled by forthcoming high-resolution Bepi-Colombo observations.

We thank Dr. Rongsheng Wang and Dr. Meng Zhou for valuable discussions. This work was supported by the B-type Strategic Priority Program of the Chinese Academy of Sciences (grant No. XDB41000000), the Strategic Priority Research Program of Chinese Academy of Sciences (grant No. XDA17010201), and the National Natural Science Foundation of China (41874198, 41674178, 41874200, 41621004). L.C. Lee was supported by the Science and Technology Development Fund (FDCT) of Macau (0035/2018/AFJ). The MESSENGER data used here are available from the Planetary Data System (https://pds-ppi.igpp.ucla.edu/).

ORCID iDs

J. Zhong https://orcid.org/0000-0003-4187-3361
L. C. Lee https://orcid.org/0000-0001-9518-4882
J. S. He https://orcid.org/0000-0001-8179-417X
H. Zhang https://orcid.org/0000-0002-3680-4989

References

Anderson, B. J., Acuña, M. H., Lohr, D. A., et al. 2007, SSRv, 131, 417
Anderson, B. J., Johnson, C. L., Korth, H., et al. 2012, JGRE, 117, E00L12
Andrews, G. B., Zurbuchen, T., Mauk, B., et al. 2007, SSRv, 131, 523
Daughton, W., Roytershteyn, V., Karimabadi, H., et al. 2011, NatPh, 7, 539
Drake, J. F., Swisdak, M., Schoeffler, K. M., Rogers, B. N., & Kobayashi, S. 2006, GeoRL, 33, L13105
Feng, H., Zhao, Y., Zhao, G., Liu, Q., & Wu, D. 2019, GeoRL, 46, 5
Gou, T., Liu, R., Kliem, B., Wang, Y., & Veronig, A. M. 2019, SciA, 5, eaau7004
Hasegawa, H., Wang, J., Dunlop, M. W., et al. 2010, GeoRL, 37, L16101
Imber, S. M., Slavin, J. A., Boardsen, S. A., et al. 2014, JGRA, 119, 5613
Jasinski, J. M., Slavin, J. A., Arridge, C. S., et al. 2016, GeoRL, 43, 6713
Lee, L. C., & Fu, Z. F. 1985, GeoRL, 12, 105
Lee, L. C., & Fu, Z. F. 1986, JGR, 91, 6807
Lee, L. C., Ma, Z. W., Fu, Z. F., & Otto, A. 1993, JGRA, 98, 3943
Markidis, S., Henri, P., Lapenta, G., et al. 2012, NPGeo, 19, 145
Milillo, A., Wurz, P., Orsini, S., et al. 2005, SSRv, 117, 397
Øieroset, M., Phan, T. D., Eastwood, J. P., et al. 2011, PhRvL, 107, 165007
Orsini, S., Blomberg, L. G., Delcourt, D., et al. 2007, SSRv, 132, 551
Pu, Z. Y., Raeder, J., Zhong, J., et al. 2013, GeoRL, 40, 3502
Raeder, J. 2006, AnGeo, 24, 381
Russell, C. T., & Elphic, R. C. 1978, SSRv, 22, 681
Russell, C. T., & Walker, R. J. 1985, JGR, 90, 11067
Schwadron, N. A., & McComas, D. J. 2013, ApJL, 778, L33
Slavin, J. A., Acuña, M. H., Anderson, B. J., et al. 2009, Sci, 324, 606
Slavin, J. A., DiBraccio, G. A., Gershman, D. J., et al. 2014, JGRA, 119, 8087
Slavin, J. A., Imber, S. M., Boardsen, S. A., et al. 2012, JGRA, 117, A00M06
Slavin, J. A., Lepping, R. P., Wu, C.-C., et al. 2010, GeoRL, 37, L02105
Slavin, J. A., Middleton, H. R., Raines, J. M., et al. 2019, JGRA, 124, 6613
Song, H.-Q., Chen, Y., Li, G., Kong, X.-L., & Feng, S.-W. 2012, PhRvX, 2, 021015
Tanaka, K. G., Retinò, A., Asano, Y., et al. 2008, AnGeo, 26, 2471
Walker, R. J., & Russell, C. T. 1985, JGR, 90, 7397
Wang, R., Lu, Q., Nakamura, R., et al. 2015, NatPh, 12, 263
Wang, R., Nakamura, R., Lu, Q., et al. 2017, PhRvL, 118, 175101
Wang, Y. L., Elphic, R. C., Lavraud, B., et al. 2005, JGRA, 110, A11221
Zhang, H., Kivelson, M. G., Angelopoulos, V., et al. 2012, JGRA, 117, A05224
Zhang, Y. C. 2016, NatSR, 6, 27592
Zhong, J., Pu, Z. Y., Dunlop, M. W., et al. 2013, JGRA, 118, 1904
Zhong, J., Wan, W. X., Slavin, J. A., et al. 2015a, JGRA, 120, 7658
Zhong, J., Wan, W. X., Wei, Y., et al. 2015b, GeoRL, 42, 10135
Zhong, J., Wei, Y., Pu, Z. Y., et al. 2018, ApJL, 860, L20
Zhou, M., Berchem, J., Walker, R. J., et al. 2017, PhRvL, 119, 055101
Zhou, M., Pang, Y., Deng, X., Huang, S., & Lai, X. 2014, JGRA, 119, 6177